ACS OMEGA

http://pubs.acs.org/journal/acsodf

Article

Experimental and Molecular Modeling Studies on the Complexation of Chromium(III) with the Angiotensin-Converting Enzyme Inhibitor Captopril

Shimaa A. Mahmoud, Mohamed Taha,* Eman S. H. Khaled, Walid Hamdy Hassan, Fatma I. Abo El-Ela, Ahmed A. Abdel-khalek,* and Reham A. Mohamed

Cite This: *ACS Omega* 2022, 7, 15909−15918

Read Online

ACCESS | Metrics & More | Article Recommendations

ABSTRACT: Captopril (CPT) is an inhibitor of angiotensin I converting enzyme, used as a medication for the treatment of people with high blood pressure, renal insufficiency, and cardiovascular diseases. It inhibits the angiogenesis process, vasoconstriction, and tumor metastasis. Some metal−captopril complexes exhibit antimicrobial activities. In the current work, the formation of the Cr^{III}−CPT complex was studied spectrophotometrically and potentiometrically in aqueous solution. Kinetics of Cr^{III}−CPT complex formation was spectrophotometrically studied over the pH range 3.20−4.20, at an ionic strength of 0.3 M at 30−50 °C. Cr^{III}−CPT complex formation was potentiometrically studied at 25 °C, where ligand protonation constants and complexes' overall stability constants were calculated. UV−vis absorption spectra were executed to confirm the complex formation. Density functional theory and molecular dynamics simulation were performed to search the geometries of the Cr^{III}−CPT complex. Atoms in molecules and interaction region indicator calculations are used to investigate intermolecular interactions for the formation of Cr^{III}−CPT complex. The antimicrobial activity of the CPT ligand and Cr^{III}−CPT complex on the prevention and control of environmental pathogenic bacteria, as tested on both Gram-positive *Staphylococcus aureus* (*S. aureus*) and Gram-negative bacteria *Escherichia coli* (*E. coli*) via agar disc diffusion method, assess the ability to use as an antimicrobial agent. CPT had shown good antimicrobial activity against both types of bacteria, which had increased slightly the zone of inhibition in Cr-CPT that indicates the increased efficacy due to Cr(III) antimicrobial activity via its oxidative damage to the bacterial cell wall. No previous study tested the CPT antimicrobial activity against Gram-positive ones such as *S. aureus*

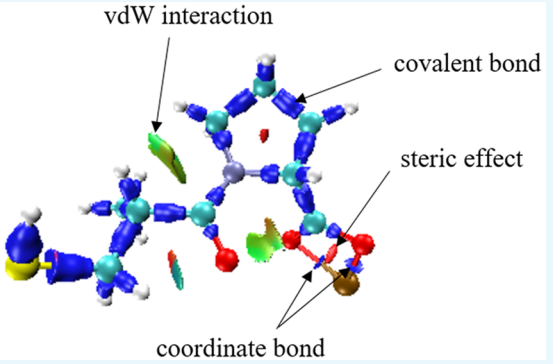

INTRODUCTION

Chromium(III) complex studies have a significant importance because of the high stability and biological activity of these complexes, especially that with amino acids which can be used as enzymatic labels.[1] Chromium is a fundamental nutritional metal that plays a role in carbohydrate, protein, and fat metabolism by potentiating the action of insulin.[2−5] Chromium deficiency has contributed to cardiovascular disease, type 2 diabetes, and metabolic syndrome.[6−8]

Captopril (CPT) is an L-proline derivative (nonessential amino acid). CPT is an inhibitor for angiotensin I converting enzyme that prevents vasodilator prostaglandin degradation, by inhibiting vasoconstriction and simulating systemic vasodilation, inhibiting the production of angiotensin II, whose levels are elevated in patients with high blood pressure.[9,10] For that reason, CPT is used as a medication for the treatment of patients with hypertension, renal insufficiency, and cardiovascular diseases.[11−14] CPT is an antioxidant and can reduce oxidative stress, which is often involved in the pathogenesis of arterial hypertension, and also decreases the cardiac inflammation associated with arterial hypertension.[15−17] Captopril represents probable therapeutic choices to stop testicular injury and dysfunction resulting from cadmium toxicity due to its anti-inflammatory and antiapoptotic activities.[18] Also, it is effective for patients with insulin-dependent diabetes who have established nephropathy and retinopathy.[19,20] CPT inhibits the growth of some types of tumors; it hinders cell proliferation in a variety of human cell types including the neuroblastoma cell line; lung fibroblasts; and mammary ductal, renal, and esophageal carcinoma cells.[21−25] Captopril intake decreases

Received: February 20, 2022
Accepted: April 15, 2022
Published: April 28, 2022

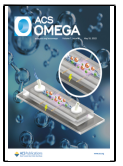

the amount of adipose tissue, increases the level of angiotensin-(1−7) in plasma, which activates phosphorylation of hormone-sensitive lipase, and may be a good candidate for weight control.[26] The maximal absorption of captopril would take place across the lipid membranes of the buccal mucosa at low pH values (pH 3 and pH 4).[27] The influence of pH on the rate of degradation of captopril in the phosphate−citrate buffer has been studied.[28] The reaction rate increased with pH and sharply so above pH 4 and, consequently, below pH 4, and deionized water was the appropriate vehicle for preparing the captopril dosage form. Lately, attention has been paid to the coordination of CPT with metal ions, the complexation of Ag(I) with captopril has been studied. The new complex formed, CPT−Ag(I), showed antimicrobial activity against different types of bacteria.[29]

Here, kinetics and the formation of the Cr^{III}−CPT complex were studied. The ligand protonation constants and complex overall stability constants were calculated potentiometrically. The proposed structure of the complex was computationally confirmed using density functional theory (DFT) and molecular dynamics (MD) simulation. The interaction between chromium(III) and CPT was investigated using the atoms in molecules (AIM) theory. The interaction region indicator (IRI) calculation is used to reveal chemical bonding and weak interaction. The ligand and metal complex have been screened for their microbiological activities against some kinds of bacteria (Gram-positive and Gram-negative).

EXPERIMENTAL SECTION

Chemicals. In experiments, chromium(III) nitrate nonahydrate (Merck, Germany) was used as a source of Cr^{3+} ions. Captopril (EIPICO, Egypt) was used as a ligand. Sodium acetate and acetic acid (Merck, Germany) were prepared and used as buffer solutions. Sodium nitrate (Fisher, USA) solution was used to maintain the ionic strength of the solutions constant during course of the reaction. NaOH and HNO_3 were from Merck.

Apparatus and Procedures of Potentiometric Titrations. A Metrohm 702 titroprocessor provided with a 700 dosino buret and a 728 magnetic stirrer was used to achieve the potentiometric titrations. The titroprocessor was connected to a computer, and the titration and data acquisition were controlled by Vesuv, version 3.0, software. The pH titrations were executed in a double-walled glass vessel connected with a thermostated water bath. The ionic strength of the solution was maintained constant at 0.1 M by adding the required concentration of sodium nitrate solution as a supporting electrolyte. The pH meter was calibrated with standard buffer solutions (pH 4.0 and 7.0) before and after each series of pH measurements, and pK_w = 13.77 at 25 °C.

For the determination of captopril protonation constants and Cr^{III}−CPT formation constants, the following solutions were prepared (total volume 40 mL) and titrated with CO_2-free sodium hydroxide solution (0.096 M) at 25 ± 0.1 °C: (1) 5.0×10^{-3} M nitric acid + 0.1 M sodium nitrate + 12.5×10^{-4} M CPT; (2) solution 1 + 12.5×10^{-4} M chromium nitrate; and (3) solution 1 + 5.0×10^{-4} M chromium nitrate, where 1, 2, and 3 stand for the estimation of CPT protonation constants and 1:1 Cr^{III}−CPT and 1:2.5 Cr^{III}−CPT stability constants, respectively.

Each solution was allowed to equilibrate for about 20 min at 25 ± 0.1 °C preceding the titration and frequently at least three times and used for fitting. The data were recorded at constant volume increments of 0.05 mL, forming real-time titration curves. The solution of sodium hydroxide was standardized with standard potassium hydrogen-phthalate. No calculations have been executed after precipitation.

Calculations of Ligand Protonation Constants and Cr^{III}-Ligand Stability Constants. The potentiometric data and the species distribution diagram (SDD) of the formed complexes in the solution were analyzed with the Hyperquad 2008[30] package to compute captopril protonation constants and Cr^{III}−ligand formation constants. The SDD is a powerful visualization tool for the accurate assessment of all species present in solution and their concentrations as a function of pH. This program simplifies visual interpretations of refinement, which helps in obtaining the best fit for the titration data. The program calculates formation constants from potentiometric data by a linear least-squares curve-fitting analysis. The stability constants are reported as β_{MLH}, where M, L, and H designate Cr^{III}, CPT, and H^+, respectively.

Calculations of complex stability which gave the best fit to the experimental data with Hyperquad are determined by minimizing the error squares sums of the potentials:

$$U = \sum w_i (pH_{obs} - pH_{calc})^2 \quad (1)$$

where w_i represents a statistical weight assigned to each point of the titration curve and pH_{obs} and pH_{calc} refer to the measured and the calculated pH values, respectively. The calculated pH was calculated automatically by Hyperquad during the refinement cycle of the calculated complexation model. In the Hyperquad software, the minimizing error squares were expressed as a sigma parameter. The sigma parameter measures the goodness of statistical fitting of the experimental to calculated model. Additionally, it was expected that the standard deviations of the calculated overall formation constants ($\log\beta_{pqr}$) should be less than the 0.5 log unit.

Kinetic Studies. The reaction rate was determined by observing the products' absorbance as a function of time. UV−vis absorption spectra of Cr^{III}−CPT complex formation was spectrophotometrically monitored for a fixed period of time with a UV−vis Jasco 530 spectrophotometer.

Kinetic studies were executed via mixing thermostated solutions of captopril at the desired pH with Cr^{III}. The pH measurements were executed with a Jenway pH meter fitted with a glass calomel electrode. Complexation of Cr^{III}−CPT was followed at 572 nm using a thermostated Jenway 6315 spectrophotometer. Pseudo-order conditions were preserved where there was at least a 10-fold excess of captopril to Cr^{III}.

Computation Details. Density functional theory calculations were used to support our experimental results. The Gaussian 09W program[31] was used to predict the molecular structure and energies of the Cr^{III}−CPT complex. DFT geometric optimization was executed in the gas phase using the B3LYP method with basis set 6-31+G (d). The correction to zero-point vibration energy was considered in the calculations of the Cr^{III}−CPT binding energy.

MD simulation of the formation of the Cr^{III}−CPT complex in aqueous solution was carried out by using the Materials Studio (BIOVIA, 2017) package. Two MD simulation systems were studied: one contains five molecules of Cr^{III} ions and five molecules of captopril ions in 1000 H_2O molecules, and the other contains five Cr^{III} ions and 10 captopril ions in 1000 water molecules. All molecules were placed randomly in the simulation box. These systems are simulated with *NPT*

https://doi.org/10.1021/acsomega.2c00986
ACS Omega 2022, 7, 15909−15918

ensemble under pressure (0.1 MPa) for 100 ps, followed by the *NPT* ensemble for 1000 ps at 25 ± 0.1 °C. The MD simulation was computed with the COMPASS II force field, and its charges were assigned. The temperature and pressure of the simulation systems were controlled by a Nosé thermostat and Berendsen barostat, respectively. The convergence tolerance quality of optimization was ultrafine. The summation method of van der Waals interaction and electrostatic forces were atom-based and Ewald, respectively. The g(r)-RDF tool was used to calculate the radial distribution functions.

Additionally, we used AIM theory[32] to investigate topological properties within the optimized structure of the Cr^{III}−CPT complex at the B3LYP/6-31+G(d) level. The total electron density (ρ), its Laplacian ($\nabla^2 \rho$), and the electronic energy density (H) at a corresponding bond critical point (BCP) are employed to identify the nature of chemical bond interactions. In general, $\rho > 0.20$ au is in a covalent interaction, and < 0.20 au is in a coordinate and closed-shell interaction (ionic, van der Waals, hydrogen bonding, etc.). The Laplacian of electron density, which is the trace of the Hessian, also determines the interaction type. A negative sign for the Laplacian of electron density signifies covalent interactions, and its positive sign stands for coordinate and closed-shell interactions. Furthermore, the electronic energy density (H) composed of electronic potential energy density (V) and electronic kinetic energy density (G) at a BCP is a more appropriate index to understand interactions. The sign of electronic energy density at a BCP determines whether the interaction is a closed shell interaction ($H > 0$) or a covalent and coordinate interaction ($H < 0$).

Also, IRI calculations are used to reveal chemical bonding and weak interaction in a Cr^{III}−CPT system. The AIM and IRI calculations were implemented in Multiwfn version 3.8.[33] Isosurface maps were rendered by VMD 1.9.4 software.[34]

Antimicrobial Activity Testing of Zn−Al LDH/GA Using a Disc-Diffusion Assay. Fifty discs of a Whitman filter paper of standard size (80 mm diameter) were used then kept in six screw-capped bottles, and to ensure sterilization, the screw-capped bottles were placed in a hot air oven for 30 min at 150 °C. The sterilized discs were impregnated overnight with the tested concentrations of both CPT and Cr-CPT at concentrations of 5 mg/mL. The paper disks were soaked at concentrations of 5 mg/mL. Isolated bacteria at a concentration of 10^8 CFU mL^{-1} were diluted in normal saline tubes according to a McFarland reference of 0.5. Thereafter, 100 μL diluted tubes were inoculated on Mueller−Hinton agar plates. The impregnated discs were placed aseptically with sterile forceps on Mueller−Hinton agar plates. All agar plates were inculcated at 37 °C for 24 h. Then, the inhibition zone diameter of all tested bacteria was determined via 2-fold serial dilution. This method was done according to CLSI[35] and Perez et al.[36] The standard strain *S. aureus* (ATCC 25923), indicative for Gram-positive bacteria, and *E. coli* (ATCC 25922), indicative for the Gram-negative ones, were used in this study.

RESULTS AND DISCUSSION

Protonation Constants. Captopril protonation constants were computed with Hyperquad from the potentiometric pH profile of the CPT solutions in the absence of chromium(III) ions. Raw data for each titration were treated with a nonlinear least-squares refinement, where optimized Hyperquad fitted the model titration curve in Figure 1a (line curve) to the experimental data (symbols) based on a least-squares analysis

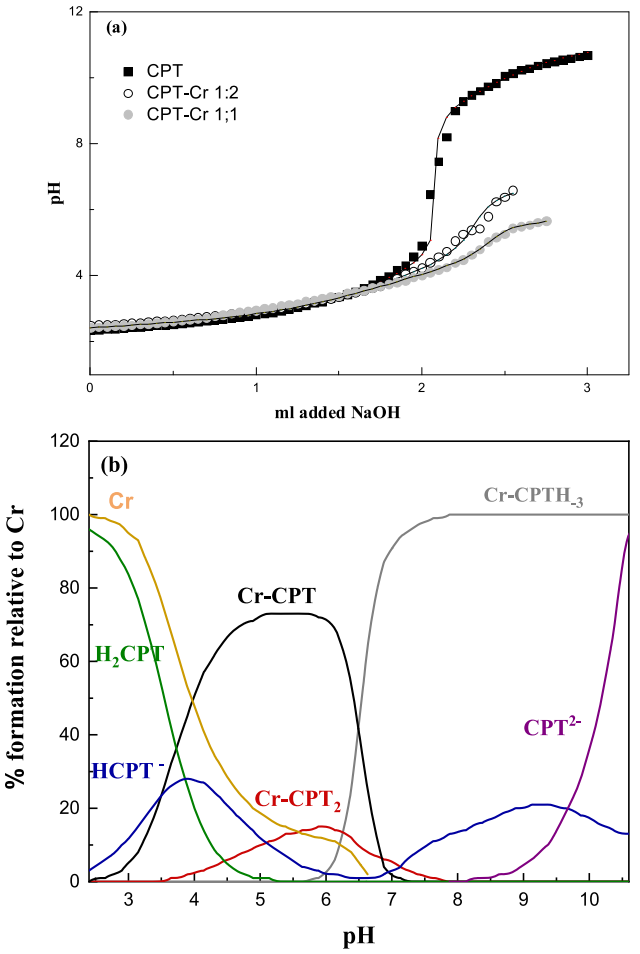

Figure 1. Potentiometric titration curve for the Cr^{III} + captopril (CPT) system at I = 0.1 M and T = 25 ± 0.1 °C. The symbol and solid lines represent the experimental and calculated data, respectively. (■) 12.5 × 10^{-4} M CPT, (○) 5 × 10^{-4} M Cr (III) + 12.5 × 10^{-4} M CPT, (●) 12.5 × 10^{-4} M Cr(III) + 12.5 × 10^{-4} M CPT. (b) Species distribution diagram for the Cr^{III} + captopril (L); $[Cr^{III}]/[L]$ = 1:2.5 at $[Cr^{III}]$ = 5 × 10^{-4} M, I = 0.1 M, and T = 25 ± 0.1 °C. Percentages are calculated with respect to the analytical concentration of the metal ion.

of K_{a1} and K_{a2}. There is a very good match of the calculated model for the experimental titration curve. The overall protonation constants, β_n, of CPT can be described as

$$\beta_n = K_1 \ldots K_2 = \frac{[H_n \mathrm{CPT}^{n-2}]}{[H^+]^n [\mathrm{CPT}^{-2}]} \quad (2)$$

where $K_1 \ldots K_2$ define the stepwise CPT dissociation constants.

The overall (log β_{pqr}) and successive (log K) protonation constants of CPT as calculated by the Hyperquad software are listed in Table 1. The symbols p, q, and r were used as the coefficients for Cr^{III}, protons, and ligands, respectively, to designate the stoichiometry associated with the possible equilibria in solution. The pK_a values for the two ionizable protons of CPT were calculated as 3.85 and 9.68. They are fairly consistent with the reported data in the literature,[37] where the pK_a values are 3.48 and = 9.68. Cr^{III}−CPT stability constants

The overall formation constants (log β_{pqr}) for the systems containing the metal ion Cr^{III} and CPT as ligand, with a molar ratio of Cr^{III} to CPT 1:1 and 1:2.5, were computed from the

https://doi.org/10.1021/acsomega.2c00986
ACS Omega 2022, 7, 15909−15918

Table 1. CPT Protonation Constants log β_{pqs} and the Overall Formation Constants for Cr^{III}–CPT Systems at I = 0.1 M and at 25 ± 0.1 °C

species	p	q	r	log β_{pqr}	SD[a]
CPT					
[HCPT]	0	1	1	9.68	0.05
[H_2CPT]	0	2	1	13.53	0.08
CPT complexes					
$[Cr^{III}(CPT)]^{2+}$	1	0	1	8.34	0.04
$[Cr^{III}(CPT)_2]^{+}$	1	0	2	15.21	0.11
$[Cr^{III}(CPT)H_{-3}]$	1	−3	1	−9.21	0.10

[a]Standard deviation.

potentiometric titration data (Tables 1). The overall reactions can be represented by the following general equation:

$$p\mathrm{Cr(III)} + q\mathrm{H} + r(\mathrm{CPT}) \rightarrow \mathrm{Cr(III)}_p\mathrm{H}_q(\mathrm{CPT})_r,\ \beta_{pqr} = \frac{[\mathrm{Cr(III)}_p\mathrm{H}_q(\mathrm{CPT})_r]}{[\mathrm{Cr(III)}]^p[\mathrm{H}]^q[\mathrm{CPT}]^r} \quad (3)$$

where p, q, and r are the coefficients for Cr^{III}, H^+, and captopril, respectively, and the square-bracket symbol refers to molar concentration. The p, q, and r values are zero or positive integers. The formation constant of the hydroxo complex was taken into account and represented by a negative value for q in Table 1. The value of the Cr^{III}–CPT complex's overall stability constant is high, showing that CPT forms strong complexes with the Cr^{III} ion.

Calculation of the stepwise formation constants (log K) was executed to show the strength of bonding between Cr^{III} and captopril. The values of log K Cr(CPT) and log K $Cr(CPT)_2$ are 8.34 and 6.87, respectively, where log K Cr(CPT) = log β101 and log K $Cr(CPT)_2$ = log β102 − log β101. The value of log K Cr(CPT) > log K $Cr(CPT)_2$ shows that the chromium ion binds more strongly with one captopril molecule.

The species distribution diagram of the $Cr(CPT)_x(OH)_y$ system at a 1:2.5 metal-to-ligand molar ratio as a function of pH and is presented in Figure 1b. The analysis of SDD for the $Cr(CPT)_x(OH)_y$ system shows that the formation of [Cr-CPT]$^+$ starts from pH 2.4 and dominates in the solution at pH 5 and begins to be negligible at pH 7.0 onward. [Cr-$(CPT)_2$]$^+$ species start to form at pH 3.6, are at a maximum at pH 5.88, and begin to be negligible at pH 7.7 onward. The formation of [$Cr(CPT)(OH)_3$] begins to be significant from pH 6 onward, reaching a maximum concentration of 100%, at pH = 7.87.

Kinetics Study on the Complexation of Cr^{III} with CPT. Cr^{III}–captopril complex formation is confirmed using UV–vis absorption. The Cr^{III}–CPT absorption spectra at a particular pH value are presented in Figure 2. It shows that, after the mixing of CPT with Cr^{III}, the absorbance increased with time over the whole wavelength range and that the two peaks of chromium nitrate at λ = 580 and 410 were shifted to λ = 572 and 408; the color changes from green to violet, proving the complexation between Cr^{III} and CPT.

The rate of the reaction was followed under pseudo-first-order conditions. Values of the observed pseudo-first-order rate constants, k_{obs}, were determined from the slopes of plotting $-\ln(A_\infty - A_t)$ vs time, t, where A indicates the measured absorbance and the subscripts refer to the time of

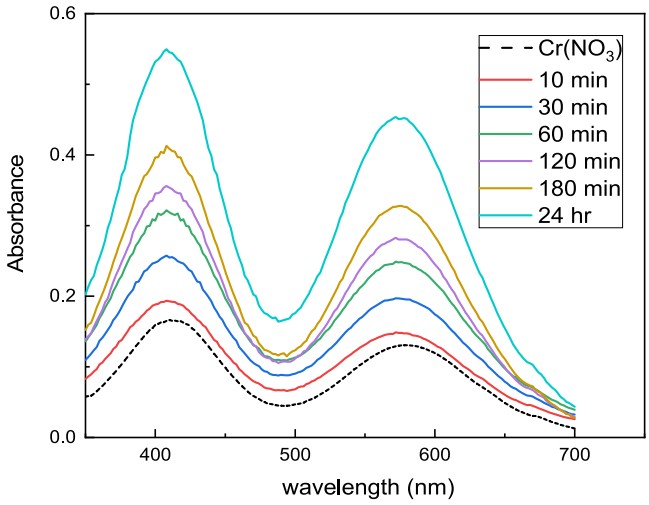

Figure 2. Spectra of Cr^{III}–CPT mixture at different times after mixing; [Cr^{III}] = 0.01 M, [CPT] = 0.1 M, I = 0.3 M, pH = 3.65, T = 25 °C.

reaction. The absorbance (A_∞) was obtained after completion of the reaction. These plots were linear for more than 97% of the reaction progress.

Variations of the first-order rate constant (k_{obs}) at constant [CPT] = 0.03 M, I = 0.30 M, pH = 3.65, and T = 35 °C over [Cr^{III}] range (1.0–8.0) × 10^{-3} M are listed in Table 2; the

Table 2. Variation of k_{obs} with Cr^{III} Concentrations and Ionic Strength at [CPT] = 0.03 M, pH = 3.65, T = 35°C

10^3 [Cr^{III}](M)	I (M)	10^3 k_{obs} (s^{-1})
1.0	0.30	4.30 ± 0.16
2.0		4.24 ± 0.11
3.0		4.25 ± 0.09
4.0		4.29 ± 0.06
5.0		4.10 ± 0.10
6.0		4.31 ± 0.05
7.0		4.31 ± 0.05
8.0		4.10 ± 0.04
3.0	0.10	4.47 ± 0.05
	0.30	4.25 ± 0.13
	0.50	4.07 ± 0.10
	0.70	4.53 ± 0.16
	0.90	4.39 ± 0.17
	1.00	4.53 ± 0.19

results indicate that the reaction is first-order dependent on the concentration of Cr^{III}, as there is no significant change in the values of k_{obs} when the concentration of Cr^{III} was varied, as described by eq 4:

$$\text{rate} = k_{obs}[\mathrm{Cr(III)}]_T \quad (4)$$

Plotting of log R vs log[Cr(III)] is a straight line with a slope (n) that equals 1.01 with a correlation coefficient of 0.9992, indicating the first-order dependence of the reaction on chromium(III) concentration. The values of first-order rate constant k_{obs} at different temperatures show that the reaction is dependent on [CPT] (Figure 3). Figure 3 shows that k_{obs} varies linearly with [CPT]/[H^+] without an intercept and obeys the relation

$$k_{obs} = k'[\mathrm{CPT}]/[\mathrm{H}^+] \quad (5)$$

https://doi.org/10.1021/acsomega.2c00986
ACS Omega 2022, 7, 15909−15918

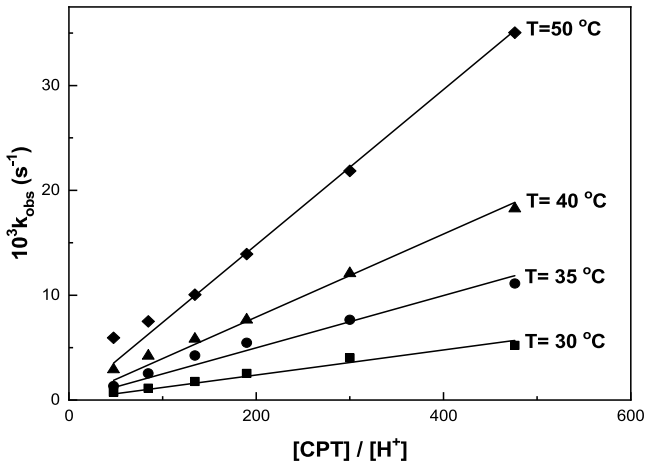

Figure 3. Variation of k_{obs} with $[CPT]/[H^+]$ at pH range 3.20−4.20 $[Cr(III)]$ = 0.03 M, T = 30−50 °C.

A plot of k_{obs} versus $[CPT]/[H^+]$ was used to find the form of the reactive species between the CPT and Cr^{III}. Figure 3 is linear, proposing that the deprotonated ligand reacts with $[Cr^{III}(H_2O)_6]^{3+}$ or the protonated ligand reacts with $[Cr^{III}(H_2O)_5(OH)]^{2+}$.

Under constant reaction conditions and various temperatures, the pH effect on the reaction rate was studied in the 3.20−4.20 pH range (Table 3). The obtained results indicate that the rate of the reaction increases with decreasing the hydrogen ion concentration.

Table 3. Kinetic Data for the Reaction of Cr^{III} with Captopril at Different Temperatures and pH's; $[Cr^{III}]$ = 0.003 M, I = 0.30 M, [CPT] = 0.03 M

	$10^3 k_{obs}$ (s^{-1})			
pH	T = 30 °C	T = 35 °C	T = 40 °C	T = 50 °C
3.20	0.73 ± 0.01	1.34 ± 0.03	3.46 ± 0.08	8.03 ± 0.23
3.45	1.13 ± 0.02	2.55 ± 0.05	5.28 ± 0.16	11.92 ± 0.20
3.65	1.77 ± 0.03	4.25 ± 0.13	7.40 ± 0.23	17.12 ± 0.29
3.80	2.55 ± 0.03	5.46 ± 0.10	9.79 ± 0.30	21.66 ± 0.31
4.00	4.03 ± 0.05	7.66 ± 0.23	12.52 ± 0.40	43.75 ± 0.17
4.20	5.21 ± 0.14	11.11 ± 0.33	17.04 ± 0.44	49.28 ± 0.14

Results in Table 2 show that k_{obs} is unaffected by changing the ionic strength of the medium in range of 0.1−1.0 M, indicating that the reaction is proceeding between charged $(Cr(H_2O)_5(OH)^{2+})$ and uncharged species (captopril).

The dependence of k_{obs} on hydrogen ion concentration can be described by the following equilibrium according to a value of K_a of 1.31 × 10^{-4} M.[38]

$$[Cr(H_2O)_6]^{3+} \Leftrightarrow [Cr(H_2O)_5(OH)]^{2+} + H^+ \quad (6)$$

The form of chromium that reacts with CPT is $[Cr(H_2O)_5(OH)]^{2+}$ since it is more reactive than $[Cr(H_2O)_6]^{3+}$ species due to the existence of the hydroxyl group, which increases the water labilities due to its π-bond ability.[39,40]

From the proposed mechanism (Scheme 1), the reaction rate is given by

$$\text{Rate} = k[CPT][Cr(H_2O)_5(OH)^{2+}] \quad (7)$$

$$= kK_a[CPT][Cr(H_2O)_6{}^{3+}]/[H^+] \quad (8)$$

$$k_{obs} = kK_a[CPT]/[H^+] \quad (9)$$

The suggested rate law presented in eq 9 is in agreement with the experimental law in eq 5, in which $k' = kK_a$. Using the value of K_a obtained potentiometrically (K_a = 3.26 × 10^{-4} M), values of 10^2k at T = 35 °C calculated from eq 9 and Figure 3 are 3.66, 7.64, 12.14, and 22.7 s^{-1}, respectively, at 30, 35, 40, and 50 °C.

Captopril reacts with $[Cr(H_2O)_5(OH)]^{2+}$, developing the inner sphere complex Cr^{III}−CPT in the rate determining step, where chromium forms a bond with CPT through the oxygen of the carboxylic group. The previous step is followed by a very rapid protonation equilibrium, which favors the aqua species, followed by another bond formation between Cr^{III} and the second oxygen of ligand carboxylate group, forming the final complex.

Calculated thermodynamic activation parameters ΔH^* and ΔS^*, from an Eyring equation plot, were found to be 69.48 ± 9 kJ/mol and −108.74 ± 3 J/K mol, respectively. The negative entropy value and the positive enthalpy value support the associative mechanism. The same isokinetic temperature was acquired from the isokinetic plot for the $[Cr(H_2O)_6]^{3+}$ with different ligands (Figure 4) backing the associative mechanism. For water substitution in $[Cr(H_2O)_6]^{3+}$ by anthranilic acid,[41] tryptophan,[42] L-lysine,[43] glycine,[44] valine,[45] and captopril [this work].

Scheme 1. Proposed Mechanism of Chromium−Captopril Complex Formation

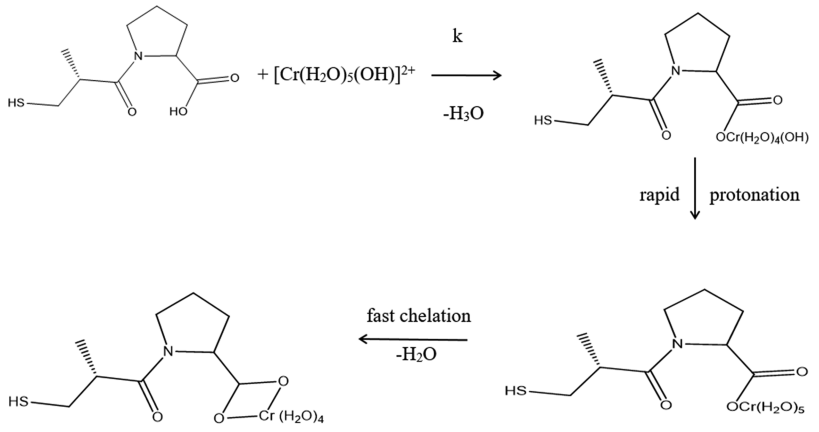

https://doi.org/10.1021/acsomega.2c00986
ACS Omega 2022, 7, 15909−15918

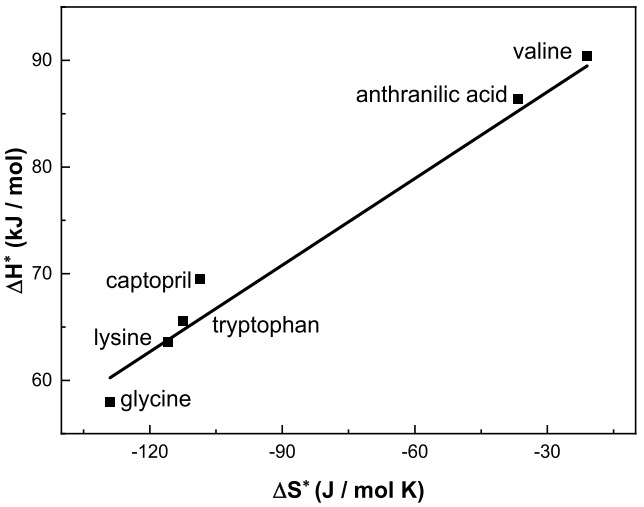

Figure 4. Isokinetic plot for water substitution in $[Cr(H_2O)_6]^{3+}$ by different ligands.

Computational Study on the Complexation of Cr^{III} with CPT. Figure 5 shows the optimized structure of the Cr^{III}−CPT complex with the B3LYP method with the 6-31+G(d) basis set. Density functional theory calculations for the complexation between chromium and captopril ions demonstrated that the complexation takes place over the oxygen atoms of the captopril carboxylate group and chromium atom. The optimized structure shown in Figure 5 has no negative vibrational force constant, indicating that it is a ground state compound. The binding energy (ΔE_{bind}) for the Cr^{III}−CPT complex equals −1178.3313 kcal/mol.

MD simulation for the complexation of CPT with Cr^{III} was simulated in water molecules to explore their complexation in aqueous solution. Figure 6 displays the MD snapshots taken at the end of the simulation of Cr^{III}/CPT 1:1 and 1:2 systems. This figure shows that the coordination between Cr^{III} and CPT takes place via the oxygen atoms of the captopril carboxylate group. A variety of hydrogen bond formations with four or more water molecules were detected at a distance of 0.35 nm from captopril.

The radial distribution function (RDF) obtained from the MD simulation provides further characterization of the possible interaction sites between different atoms to identify the complexation reaction. Figure 7 shows the RDF of Cr···O=C, Cr···$O_{nitrate}$, Cr···S, Cr···OW, $O_{nitrate}$···HW, C=O···HW, and SH···OW, where HW and OW are hydrogen and oxygen atom of water, respectively. MD simulation of the Cr^{III}−CPT system shows that the chromium atom forms three bonds: a strong coordinate bond with the oxygen atoms of the CPT carboxylate group as shown in Cr···O=C RDF, which has a peak at 2.11 Å, with the oxygen atom of water molecules as shown in the Cr···OW at 2.39 Å and with oxygen atoms of nitrate as shown in the Cr···$O_{nitrate}$ at 2.15 Å. The intense peak between chromium and nitrate proposes the formation of the complex in neutral form.

Hydrogen bond formation in the Cr^{III}−CPT complex is characterized in the RDF (C=O····HW) and ($O_{nitrate}$···HW), where hydrogen bonds are formed between the oxygen atoms of the CPT carboxylate group and hydrogen atoms of H_2O, as displayed in the O=C····HW RDF at 1.55 Å, and between the oxygen atom of nitrate and hydrogen atoms of H_2O ($O_{nitrate}$···HW) at 1.57 Å, since they are within the hydrogen bond distance.

The RDF of the chromium and sulfur atom (Cr···S) displays that the chromium ion does not form a bond with the ligand thiol group. The hydrogen atoms of the captopril thiol group do not form hydrogen bonds with oxygen atoms of H_2O molecules, as observed from the SH····OW RDFs. There is no significant change in the position of peaks formed in RDFs in the two simulated systems of the Cr^{III}−CPT (1:1) system and the (1:2) Cr^{III}−CPT system. The results obtained from the MD simulation confirm the formation of the Cr^{III}−CPT complex. Kinetics and potentiometric studies confirm the formation of 1:1 Cr^{III} to captopril.

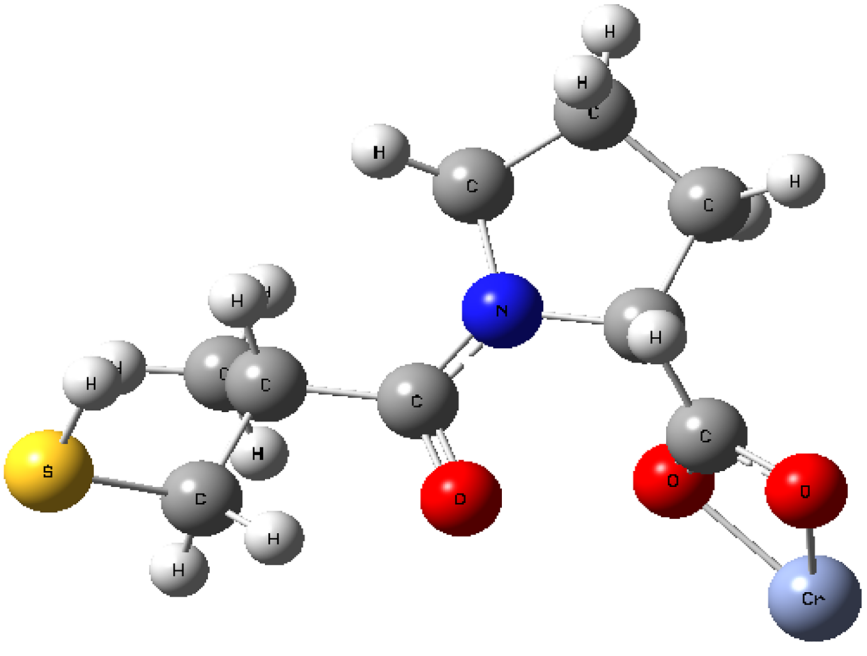

Figure 5. Cr^{III}−CPT complex optimized structure using DFT.

https://doi.org/10.1021/acsomega.2c00986
ACS Omega 2022, 7, 15909−15918

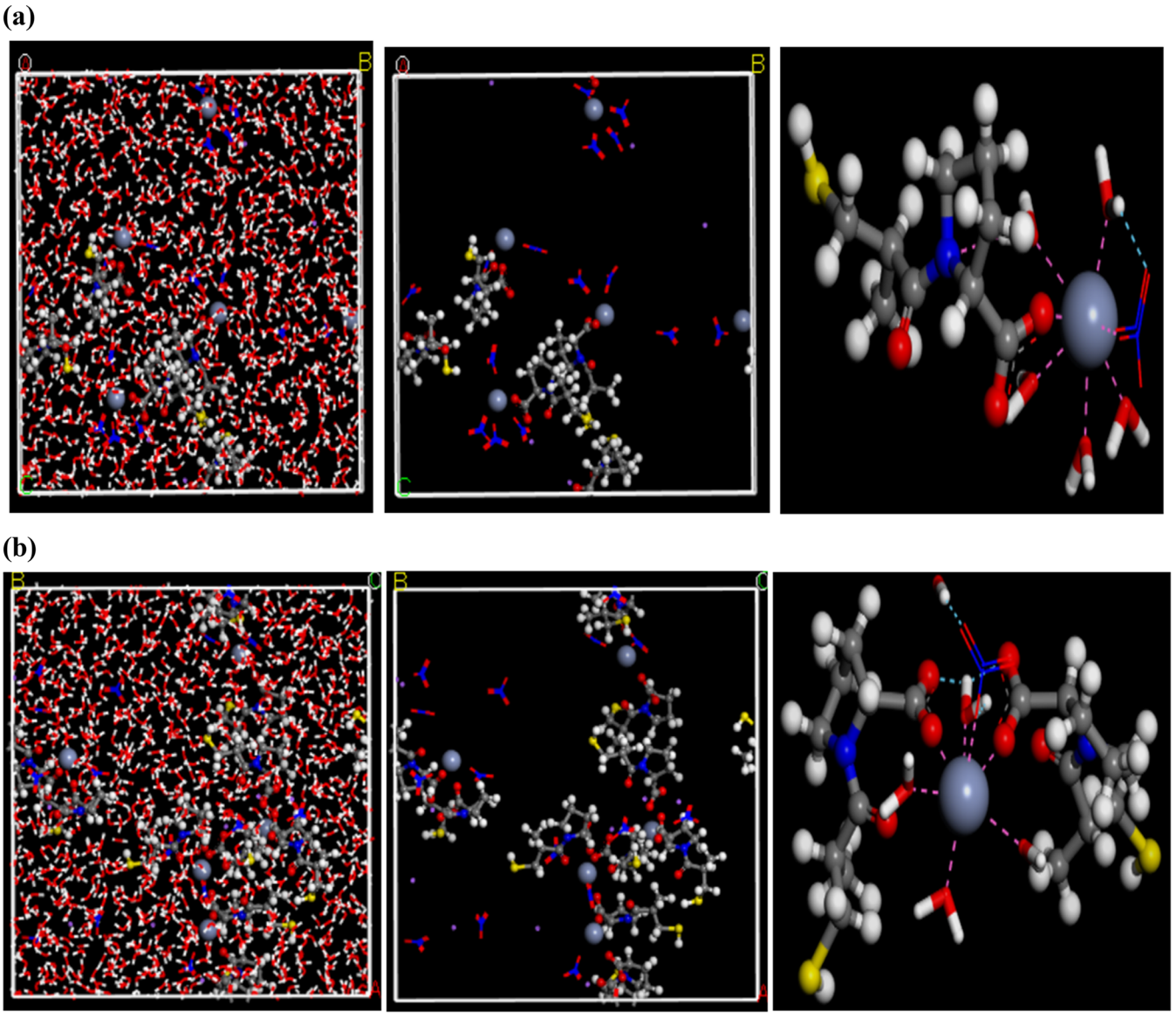

Figure 6. MD snapshots of CPT (dark gray), Cr^{III} (gray), and water (red) molecules taken from simulations for Cr^{III} + CPT + nitrate + sodium + water system (a) 1:1 Cr^{III}/CPT and (b) 1:2 Cr^{III}/CPT.

Figure 8 shows the critical points (CPs) in the optimized structure of the Cr^{III}−CPT complex. The topological parameters of the interaction between chromium and oxygen atoms of the captopril carboxylate group were analyzed from the optimized structure at the B3LYP/6-31+G(d) level (Table 4). It is observed that the values of ρ are lower than 0.2 au, $\nabla^2\rho > 0$, and $H < 0$, indicating that the interactions between Cr^{III} and CPT are coordinate bonds, where chromium ions form two coordinate bonds with the two oxygen atoms of the captopril carboxylate group. The topological analysis of electron density provides evidence for the existence of intramolecular interactions between Cr^{III} and CPT.

Figure 9 presents the isosurface map of IRI = 1.0 of the Cr^{III}−CPT complex which reveals both covalent and noncovalent interaction regions. IRI isosurfaces successfully revealed the Cr−O bonds. The coordinate bonds between the Cr^{III} and coordinated oxygen atoms of CPT are exhibited by blue IRI isosurfaces. The steric effect within the five-membered pyrrole ring and the Cr−O−O ring can be identified by the red areas of the isosurfaces. The van der Waals interaction (vdW) due to the close contact between the same atoms can also be identified by the green part of the IRI isosurfaces.[46]

Antimicrobial Activity Study. The antimicrobial activity of CPT and Cr-CPT had been tested against both Gram-positive and Gram-negative bacteria via the agar disc diffusion method on treptone soya agar media. We confirmed the modest inhibitory activity of CPT and Cr^{III}−CPT against both Gram-negative bacteria *E. coli* as previously reported in the literature[47] and Gram-positive *S. aureus* that showed a more wide zone of inhibition as shown in Figure 10. Moreover, the extent of inhibition was also affected and increased in Cr^{III}−CPT than in CPT. As previous studies had reported, the CPT mechanism of action against antimicrobial activity inhibiting N-succinyl-l,l-diaminopimelic acid desuccinylase (DapE) is a metallohydrolase involved in the meso-diaminopimelate (mDAP)/lysine biosynthetic pathway necessary for lysine biosynthesis and for building the peptidoglycan cell wall of bacteria.[47] The zone of inhibition was slightly more in Gram-positive strains and in Cr^{III}−CPT. Therefore, CPT is a modest

https://doi.org/10.1021/acsomega.2c00986
ACS Omega 2022, 7, 15909−15918

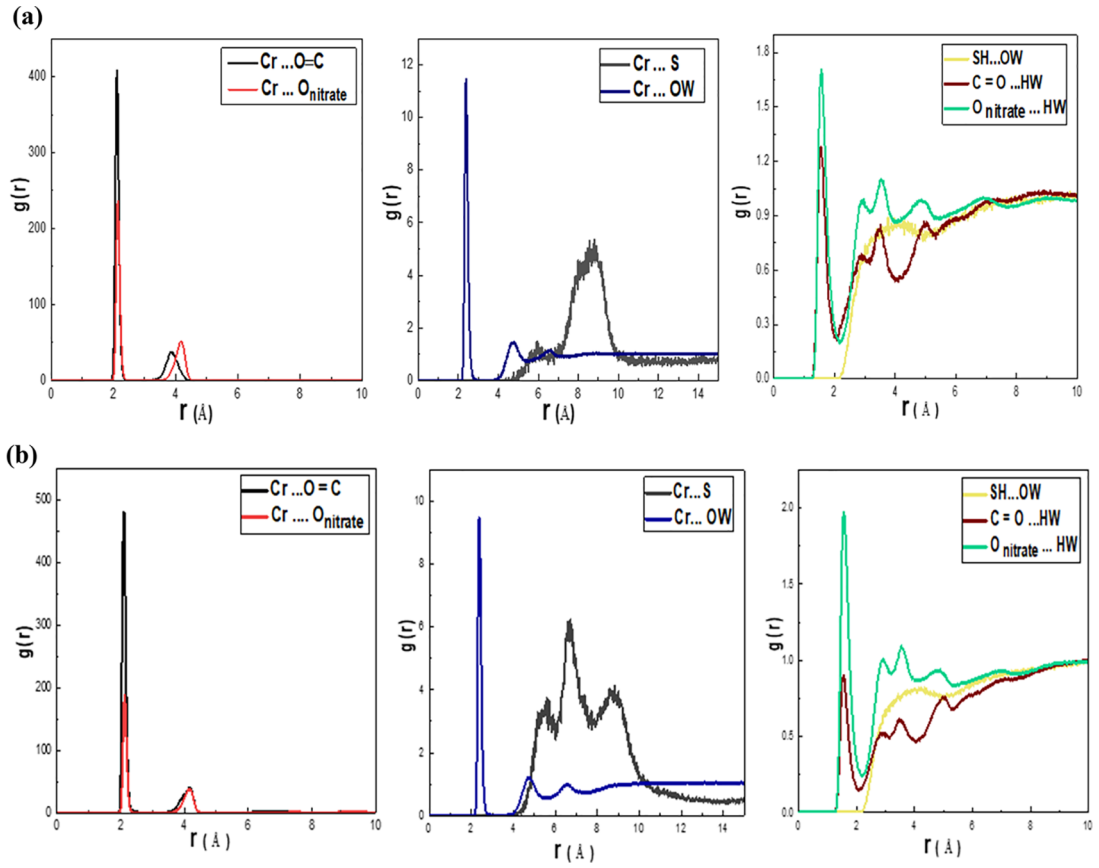

Figure 7. RDFs acquired from MD simulation of Cr^{III}−CPT system. (a and b) 1:1 and 1:2 Cr^{III}/CPT system, respectively.

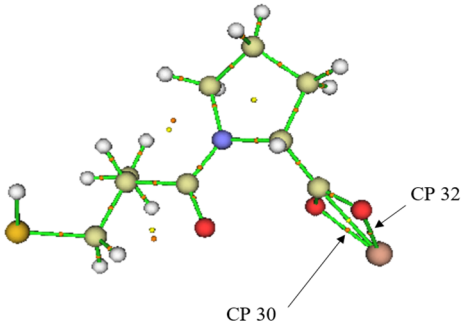

Figure 8. Critical points in the optimized structure of the Cr^{III}−CPT complex.

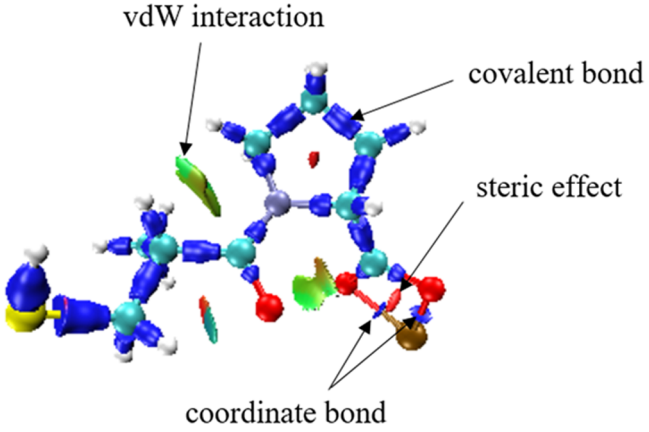

Figure 9. Isosurface map of IRI = 1.0 of the Cr^{III}−CPT system.

antibiotic, inhibiting Gram-negative bacteria at high doses, but its mechanism of action or molecular target remains unknown. Finally, considering that DapE is a promising antibiotic target, the failure of a lead compound that inhibits DapE in vitro to show any measurable anti-DapE effect in bacteria provides a sobering reminder of the difficulty of translating in vitro data to effects in vivo, even in pure microbiological cultures as had been tested in previous studies.[47]

The work described here shows that the Cr^{III}−CPT complex is bactericidal for *S. aureus* and *E. coli*. Our results indicate that Cr(III) itself may be interesting to open new paths for metallo drug chemotherapy against different bacterial genera since some of these complexes have been found to exhibit remarkable antibacterial activities. Cr(III) addition to CPT

Table 4. Selected Calculated Topological Parameters for the Intermolecular Interactions between Chromium and CPT Analyzed from the Optimized Structure at the B3LYP/6-31+G(d) Level

interaction	ρ	$\nabla^2\rho_{BCP}$	G_{BCP} (eV)	V_{BCP} (eV)	H (eV)
Cr···O CP 30	0.1052	0.5599	0.1470	−0.1540	-0.7026×10^{-2}
Cr···O CP 32	0.1097	0.5783	0.1534	−0.1623	-0.8871×10^{-2}

https://doi.org/10.1021/acsomega.2c00986
ACS Omega 2022, 7, 15909−15918

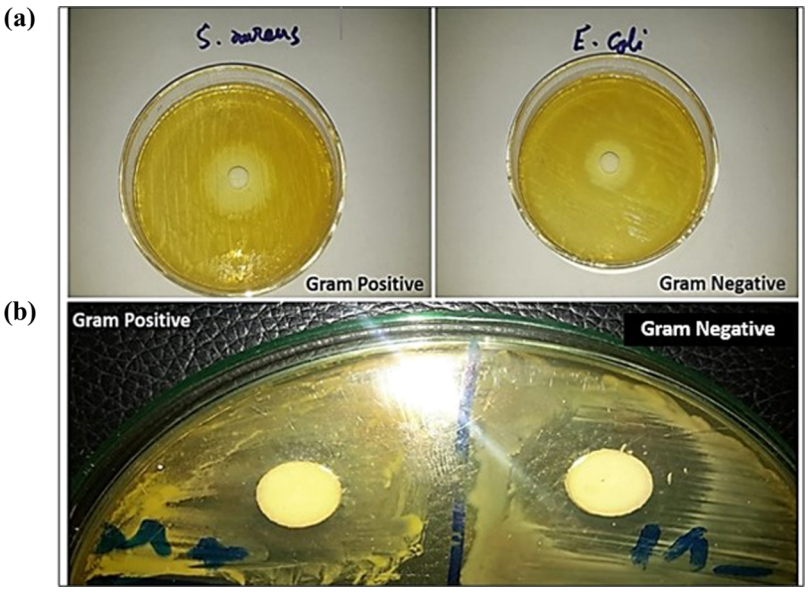

Figure 10. Diameter of inhibition zone (mm) of (a) Cr^{III}−CPT complex and (b) CPT against both Gram-positive and Gram-negative bacteria.

for complex formation had shown high antimicrobial activities against *E. coli* and *S. aureus*. In our biological experiments, by using Cr(III) we have observed high biological activity against Gram-negative and Gram-positive bacteria. The results showed that the Cr^{III}−CPT complex used in the present work inhibits the growth of bacteria to a wider extent compared to CPT alone.[48]

CONCLUSION

Here, the reaction between Cr^{III} with CPT was spectrophotometrically and potentiometrically studied in aqueous solution, where $[Cr(H_2O)_5OH^{2+}]$ is the reactive species. The reaction is first-order dependent on $[Cr^{III}]$, increasing with decreasing hydrogen ion concentration and increasing the temperature. An associative mechanism is proposed for this reaction. The calculated values of CPT protonation constants (pK_a = 3.85, 9.68) were fairly consistent with the data reported in the literature. The values of the stepwise stability constants calculated potentiometrically show that the Cr^{III}−CPT complex is more stable than Cr^{III}−CPT_2. DFT, MD simulation, IRI, and topological analysis of electron density provides evidence for the existence of chemical bonds between Cr^{III} and CPT, where chromium forms two coordinate bonds with CPT, proving the complexation between them. The Cr^{III}−CPT complex had shown high antimicrobial activities against *E. coli* and *S. aureus*. It may be concluded that the Cr^{III}−CPT complex used in the present work inhibits the growth of bacteria to a wider extent compared to CPT alone.

AUTHOR INFORMATION

Corresponding Authors

Mohamed Taha − *Materials Science and Nanotechnology Department, Faculty of Postgraduate Studies for Advanced Sciences, Beni-Suef University, 62511 Beni-Suef, Egypt*; orcid.org/0000-0002-5367-2009; Email: mtaha@psas.bsu.edu.eg

Ahmed A. Abdel-khalek − *Chemistry Department, Faculty of Science, Beni-Suef University, 62511 Beni-Suef, Egypt*; Email: ahmedakhalek41@gmail.com

Authors

Shimaa A. Mahmoud − *Chemistry Department, Faculty of Science, Beni-Suef University, 62511 Beni-Suef, Egypt*

Eman S. H. Khaled − *Chemistry Department, Faculty of Science, Beni-Suef University, 62511 Beni-Suef, Egypt*

Walid Hamdy Hassan − *Department of Microbiology Mycology and Immunology, Faculty of Veterinary Medicine, Beni-Suef University, 62511 Beni-Suef, Egypt*

Fatma I. Abo El-Ela − *Department of Pharmacology, Faculty of Veterinary Medicine, Beni-Suef University, 62511 Beni-Suef, Egypt*

Reham A. Mohamed − *Chemistry Department, Faculty of Science, Beni-Suef University, 62511 Beni-Suef, Egypt*

Complete contact information is available at: https://pubs.acs.org/10.1021/acsomega.2c00986

Notes

The authors declare no competing financial interest.

REFERENCES

(1) Okada, S.; Suzuki, M.; Ohba, H. Enhancement of ribonucleic acid synthesis by chromium (III) in mouse liver. *J. Inorg. Biochem.* **1983**, *19*, 95−103.

(2) Althuis, M. D.; Jordan, N. E.; Ludington, E. A.; Wittes, J. T. Glucose and insulin responses to dietary chromium supplements: a meta-analysis. *Am. J. Clin. Nutr.* **2002**, *76*, 148−155.

(3) Anderson, R. A. Chromium, glucose intolerance and diabetes. *J. Am. Coll. Nutr.* **1998**, *17*, 548−555.

(4) Anderson, R. A. Chromium and insulin resistance. *Nutr. Res. Rev.* **2003**, *16*, 267−275.

(5) Cefalu, W. T.; Hu, F. B. Role of chromium in human health and in diabetes. *Diabetes care* **2004**, *27*, 2741−2751.

(6) Bai, J.; Xun, P.; Morris, S.; Jacobs, D. R.; Liu, K.; He, K. Chromium exposure and incidence of metabolic syndrome among American young adults over a 23-year follow-up: the CARDIA Trace Element Study. *Sci. Rep.* **2015**, *5*, 1−8.

(7) Hummel, M.; Standl, E.; Schnell, O. Chromium in metabolic and cardiovascular disease. *Horm. Metab. Res.* **2007**, *39*, 743−751.

(8) Rajpathak, S.; Rimm, E. B.; Li, T.; Morris, J. S.; Stampfer, M. J.; Willett, W. C.; Hu, F. B. Lower toenail chromium in men with diabetes and cardiovascular disease compared with healthy men. *Diabetes Care* **2004**, *27*, 2211−2216.

https://doi.org/10.1021/acsomega.2c00986
ACS Omega 2022, 7, 15909−15918

(9) Skeggs, L. T.; Dorer, F. E.; Levine, M.; Lentz, K. E.; Kahn, J. R. The biochemistry of the renin-angiotensin system. *Adv. Exp. Med. Biol.* **1980**, *130*, 1−27.
(10) Skeggs, L. T.; Dorer, F. E.; Kahn, J. R.; Lentz, K. E.; Levine, M. The biochemistry of the renin-angiotensin system and its role in hypertension. *Am. J. Med.* **1976**, *60*, 737−748.
(11) Kostis, J. B. Angiotensin converting enzyme inhibitors. II. Clinical use. *Am. Heart J.* **1988**, *116*, 1591−1605.
(12) Hou, W. C.; Chen, H. J.; Lin, Y. H. Antioxidant peptides with angiotensin converting enzyme inhibitory activities and applications for angiotensin converting enzyme purification. *J. Agric. Food Chem.* **2003**, *51*, 1706−1709.
(13) Bhuyan, B. J.; Mugesh, G. Synthesis, characterization and antioxidant activity of angiotensin converting enzyme inhibitors. *Org. Biomol. Chem.* **2011**, *9*, 1356−1365.
(14) Cushman, D. W.; Cheung, H. S.; Sabo, E. F.; Ondetti, M. A. Design of new antihypertensive drugs: potent and specific inhibitors of angiotensin-converting enzyme. *Prog. Cardiovasc. Dis.* **1978**, *21*, 176−182.
(15) Aruoma, O. I.; Akanmu, D.; Cecchini, R.; Halliwell, B. Evaluation of the ability of the angiotensin-converting enzyme inhibitor captopril to scavenge reactive oxygen species. *Chem.-Biol. Interact.* **1991**, *77*, 303−314.
(16) Li, G. X.; Liu, Z. Q. Captopril and 6-mercaptopurine: Whose SH possesses higher antioxidant ability? *Eur. J. Med. Chem.* **2009**, *44*, 4841−4847.
(17) Miguel-Carrasco, J. L.; Monserrat, M. T.; Mate, A.; Vázquez, C. M. Comparative effects of captopril and l-carnitine on blood pressure and antioxidant enzyme gene expression in the heart of spontaneously hypertensive rats. *Eur. J. Pharmacol.* **2010**, *632*, 65−72.
(18) Fouad, A. A.; Jresat, I. Captopril and telmisartan treatments attenuate cadmium-induced testicular toxicity in rats. *Fundam. Clin. Pharmacol.* **2013**, *27*, 152−160.
(19) Lewis, E. J.; Hunsicker, L. G.; Bain, R. P.; Rohde, R. D. The effect of angiotensin-converting-enzyme inhibition on diabetic nephropathy. *N. Engl. J. Med.* **1993**, *329*, 1456−1462.
(20) Jackson, W. E.; Holmes, D. L.; Garg, S. K.; Harris, S.; Chase, H. P. Angiotensin-converting enzyme inhibitor therapy and diabetic retinopathy. *Ann. Ophthalmol.* **1992**, *24*, 99−103.
(21) Chen, L.; Re, R. N.; Prakash, O.; Mondal, D. Angiotensin-converting enzyme inhibition reduces neuroblastoma cell growth rate. *Proc. Soc. Exp. Biol. Med.* **1991**, *196*, 280−283.
(22) Nguyen, L.; Ward, W. F.; Ts' Ao, C. H.; Molteni, A. Captopril inhibits proliferation of human lung fibroblasts in culture: a potential antifibrotic mechanism. *Proc. Soc. Exp. Biol. Med.* **1994**, *205*, 80−84.
(23) Small, W.; Molteni, A.; Kim, Y. T.; Taylor, J. M.; Chen, Z.; Ward, W. F. Captopril modulates hormone receptor concentration and inhibits proliferation of human mammary ductal carcinoma cells in culture. *Breast cancer Res. Treat.* **1997**, *44*, 217−224.
(24) Hii, S. I.; Nicol, D. L.; Gotley, D. C.; Thompson, L. C.; Green, M. K.; Jonsson, J. R. Captopril inhibits tumour growth in a xenograft model of human renal cell carcinoma. *Br. J. Cancer* **1998**, *77*, 880−883.
(25) Sjoberg, T.; Garcia Rodriguez, L. A.; Lindblad, M. Angiotensin-converting enzyme inhibitors and risk of esophageal and gastric cancer: a nested case-control study. *Clin. Gastroenterol. Hepatol.* **2007**, *5*, 1160−1166.
(26) Oh, Y. B.; Kim, J. H.; Park, B. M.; Park, B. H.; Kim, S. H. Captopril intake decreases body weight gain via angiotensin-(1−7). *Peptides* **2012**, *37*, 79−85.
(27) McElnay, J. C.; Al-Furaih, T. A.; Hughes, C. M.; Scott, M. G.; Elborn, J. S.; Nicholls, D. P. The effect of pH on the buccal and sublingual absorption of captopril. *Eur. J. Clin. Pharmacol.* **1995**, *48*, 373−379.
(28) Huang, Y. B.; Tsai, Y. H.; Chang, J. S.; Liu, J. C.; Tsai, M. J.; Wu, P. C. Effect of antioxidants and anti-irritants on the stability, skin irritation and penetration capacity of captopril gel. *Int. J. Pharm.* **2002**, *241*, 345−351.
(29) Isab, A. A.; Wazeer, M. I. Solid and solution NMR studies of the complexation of Ag+ with the trans isomer of captopril: Biological activities of this high blood pressure drug along with its Ag+ complex. *Spectrochim. Acta A Mol. Biomol. Spectrosc.* **2006**, *65*, 191−195.
(30) Gans, P.; Sabatini, A.; Vacca, A. Investigation of equilibria in solution. Determination of equilibrium constants with the HYPERQUAD suite of programs. *Talanta* **1996**, *43*, 1739−1753.
(31) Frisch, M. J.; Trucks, G. W.; Schlegel, H. B.; Scuseria, G. E.; Robb, M. A.; Cheeseman, J. R.; Scalmani, G.; Barone, V.; Mennucci, B.; Petersson, G. A.; et al. *Gaussian 09*, Revision C.01; Gaussian, Inc.: Wallingford, CT, 2009.
(32) Bader, R. F. W. *Atoms in Molecules: A Quantum Theory*; Oxford University Press, Oxford, 1990.
(33) Lu, T.; Chen, F. Multiwfn: a multifunctional wavefunction analyzer. *J. Comput. Chem.* **2012**, *33*, 580−592.
(34) Humphrey, W.; Dalke, A.; Schulten, K. VMD: visual molecular dynamics. *J. Mol. Graph.* **1996**, *14*, 33−38.
(35) CLSI, Clinical and Laboratory Standards Institute. *Methods for dilution antimicrobial susceptibility tests of bacteria isolated form aquatic animal; approved guideline M49-a*; CLSI: Waune, PA, 2006.
(36) Perez, C.; Pauli, M.; Bazerque, P. An antibiotic assay by agar-well diffusion method. Acta. *Biol. Med. Exp.* **1990**, *15*, 113−115.
(37) Joshaghani, M.; Gholivand, M. B.; Mosavat, A. R. Chelation Study of Captopril with Cd^{2+} and Pb^{2+} ions. *Am. J. Biochem. and Biotechnol.* **2008**, *4*, 245−249.
(38) Basolo, F.; Pearson, R. G. *Mechanism of Inorganic Reaction*, 2nd ed.; Wiley: New York, 1958; p 608.
(39) Khan, I. A.; Kabir-ud-Din. Kinetics of anation of hexaaquachromium (III) Ion by aspartic acid: mechanism and activation parameters. *Trans. Met. Chem.* **1986**, *11*, 391−395.
(40) Campisi, A.; Tregloan, P. A. Kinetics and equilibria of Ga (III) thiocyanate complex formation. Mechanism of ligand substitution reactions of Ga (III) in aqueous solution. *Inorg. Chim. Acta* **1985**, *100*, 251−259.
(41) Tyagi, S. C.; Khan, A. A. Complex Formed by Interaction of Anthranilic Acid with Chromium (III) in Solution: A Kinetic Study. *Indian J. Chem.* **1978**, *16*, 657−660.
(42) Shahid, M.; Khan, I. A.; Kabir-ud-Din. Kinetic and mechanistic studies on the complexation of aquachromium (III) with DL-tryptophan in aqueous acidic media. *J. Chem. Soc., Dalton Trans.* **1990**, *10*, 3007−3012.
(43) Guindy, N. M.; Abou-Gamra, Z. M.; Abdel-Messih, M. F. Kinetic studies on the complexation of chromium (III) with some amino acids in aqueous acidic medium. *Monatsh. Chem.* **2000**, *131*, 857−866.
(44) Khan, I. A.; Kabir-Ud-Din. Anation of hexaaquochromium (III) by glycine. *J. Inorg. Nucl. Chem.* **1981**, *43*, 1082−1085.
(45) Khan, I. A. Kinetics of Anation of Hexaaquochromium (III) Ion by Valine in Aqueous Acidic Medium. *Indian J. Chem.* **1984**, *23*, 98−101.
(46) Lu, T.; Chen, Q. Interaction region indicator: A simple real space function clearly revealing both chemical bonds and weak interactions. *Chemistry-Methods* **2021**, *1*, 231−239.
(47) Uda, N. R.; Creus, M. Selectivity of Inhibition of N-Succinyl-l,l-Diaminopimelic Acid Desuccinylase in Bacteria: The product of dapE-gene Is Not the Target of l-Captopril Antimicrobial Activity. *Bioinorg Chem. Appl.* **2011**, 306465..
(48) Paez, P. L.; Bazan, C. M.; Bongiovanni, M. E.; Toneatto, J.; Albesa, I.; Becerra, M. C.; Arguello, G. A. Oxidative Stress and Antimicrobial Activity of Chromium(III) and Ruthenium(II) Complexes on Staphylococcus aureus and Escherichia coli. *BioMed. Research International* **2013**, 906912..

https://doi.org/10.1021/acsomega.2c00986
ACS Omega 2022, 7, 15909−15918